Electronic supplementary information

Unique Holey Graphene/Carbon Dots Frameworks by Microwave-Initiated Chain Reduction for High-Performance Compressible Supercapacitors and Reusable Oil/Water Separation

*Wenqiang Wang‡, Jie Jin‡, Yiyang Wu, Wenyi Zhang, Hao Jiang, Xingwei Li, and Gengchao Wang**

Shanghai Key Laboratory of Advanced Polymeric Materials, Shanghai Engineering Research Center of Hierarchical Nanomaterials, School of Materials Science and Engineering, East China University of Science and Technology, Shanghai 200237, P. R. China

*Prof. Geng C Wang

E-mail: gengchaow@ecust.edu.cn

‡These authors contributed equally to this work.

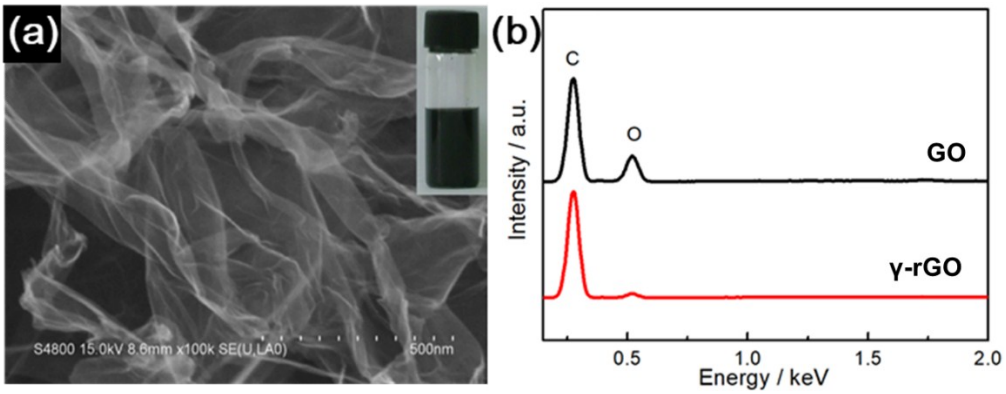

Figure S1. (a) FE-SEM image of γ-rGO (inset: the γ-rGO dispersion), (b) EDS of GO and γ-rGO.

Figure S1a shows that the as-prepared γ-rGO has good dispersion in water. From the EDS of Figure S1b, the C/O weight ratio of GO is 1.8 and that of γ-rGO is 5.4, which can be attributed to the fact that the hydrogen radicals produced by irradiation can effectively reduce the oxygen-containing groups.

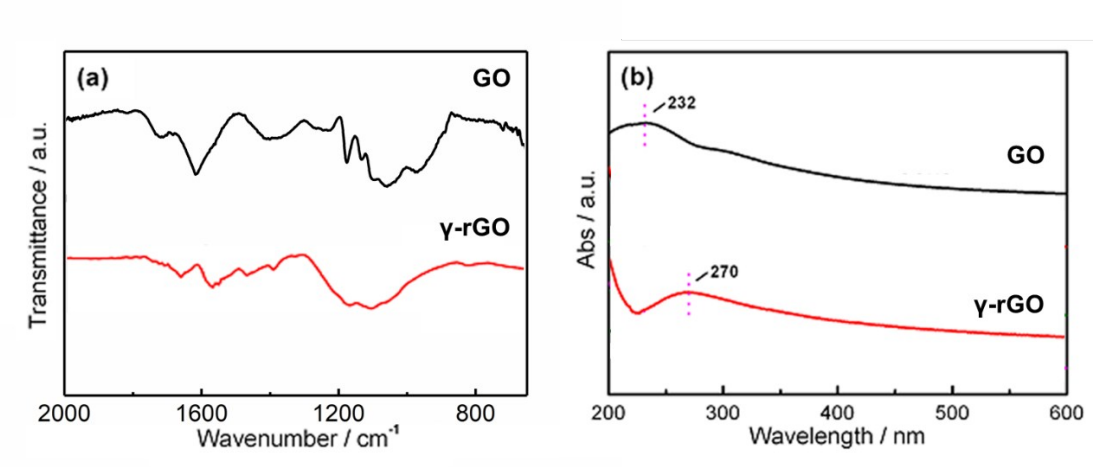

Figure S2. (a) FTIR spectra and (b)UV-Vis spectra of GO and γ-rGO.

After irradiated by ^{60}Co, the characteristic peaks of C-O (1051 cm^{-1}), C-O-C (1218 cm^{-1}), C-OH (1384 cm^{-1}), and C=O (1714 cm^{-1}) are obviously weakened (Figure S2a). From the UV-Vis spectra of Figure S2b, the peak of 232 nm (GO) red shift to 270 nm (γ-rGO), indicating that the conjugation degree is enhanced by irradiation.

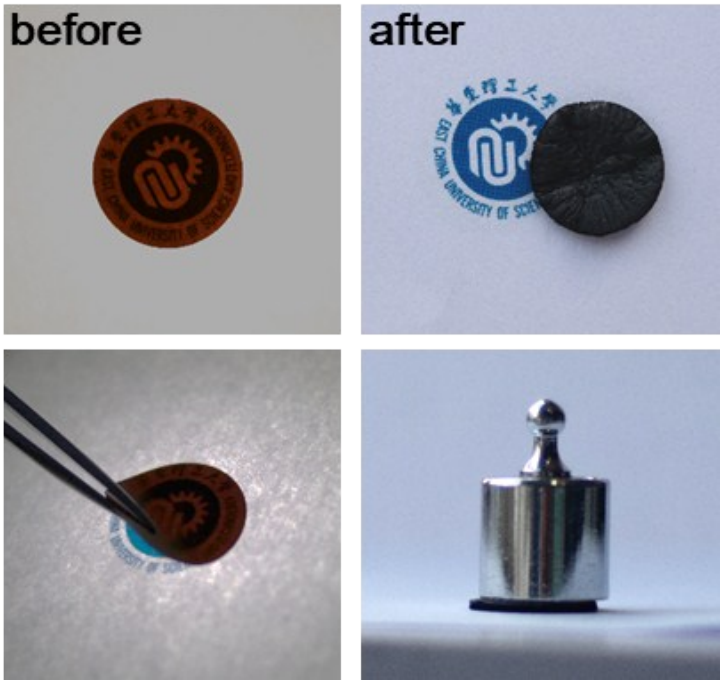

Figure S3. Photos of NPGF-30 before and after microwave treatment.

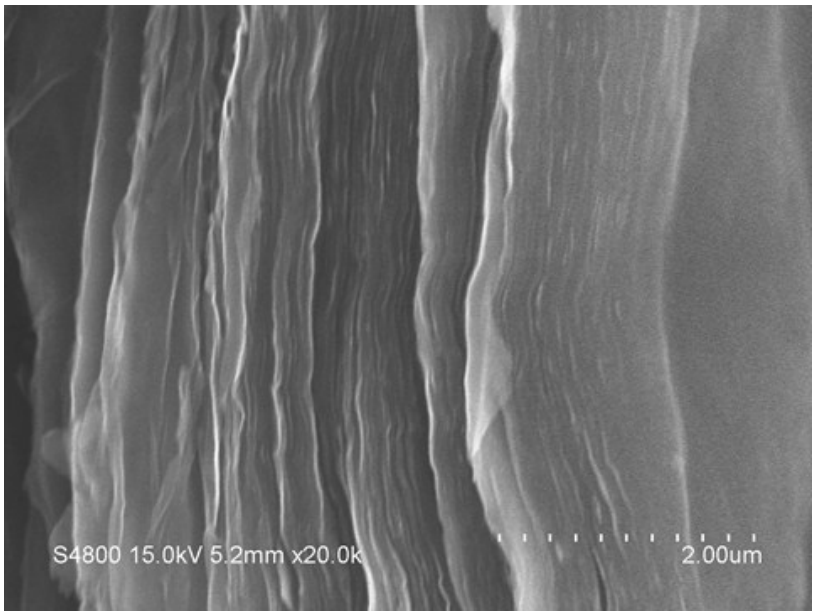

Figure S4. SEM image of GO/PVP-30 paper after microwave treatment.

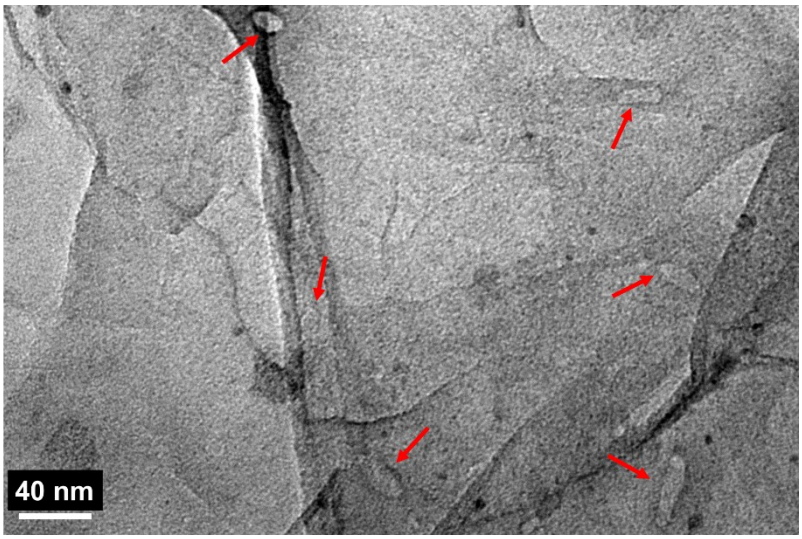

Figure S5. TEM image of the NPGF-30.

For TEM observation, the NPGF-30 was fragmented ultrasonically in ethanol and centrifuged to obtain the dispersions. From the TEM image of Figure, holes with a diameter of 20~40 nm can be observed on graphene sheets. We have noticed that the carbon dots observed in the TEM image are far fewer than those observed in the SEM image (Figure 2e), which may be due to the fact that intense ultrasound has caused the carbon dots to fall off from graphene.

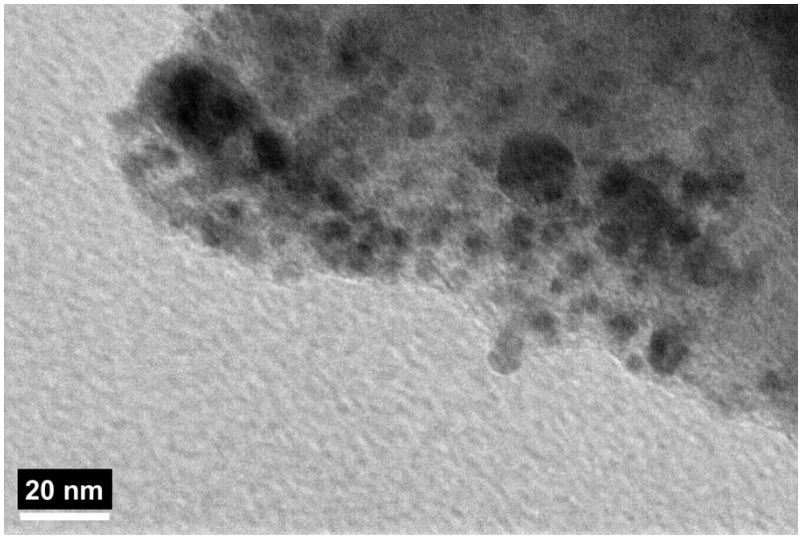

Figure S6. High-magnification TEM image of NPGF-30 focusing on carbon dots.

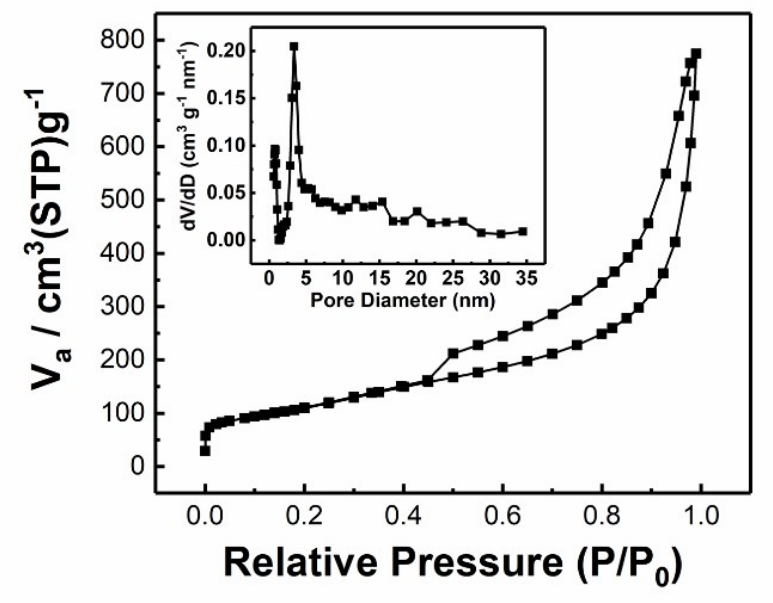

Figure S7. Nitrogen adsorption-desorption isotherm and pore distribution for NPGF-30.

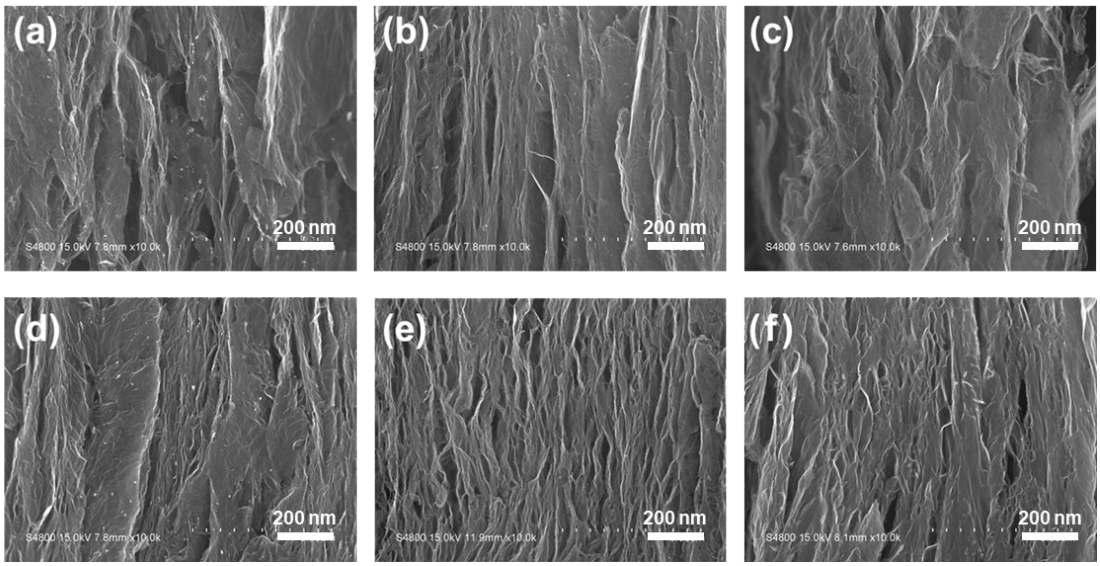

Figure S8. Cross-sectional FESEM images of NPGFs prepared with different PVP dosage: (a) 0%, (b) 5%, (c) 10%, (d) 20%, (e) 30% and (f) 40%.

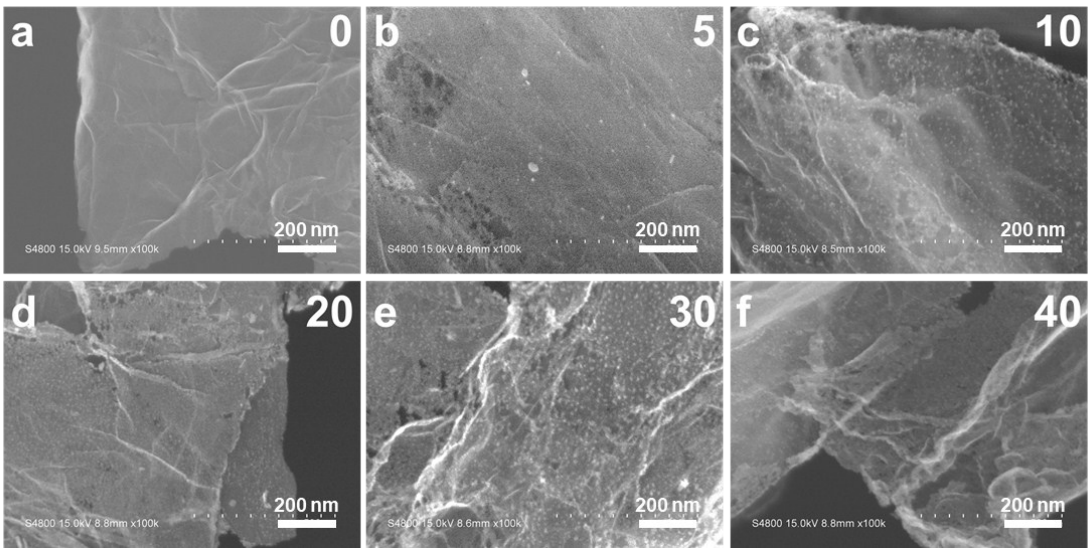

Figure S9. High-magnification FESEM images of NPGFs prepared with different PVP dosage.

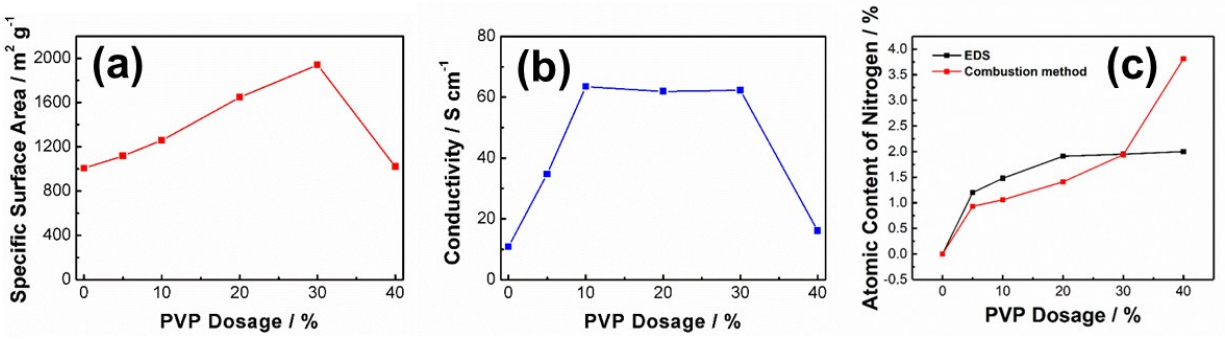

Figure S10. (a) Specific surface area (methylene blue adsorption), (b) electrical conductivity, and (c) atomic content of nitrogen prepared with different PVP dosage.

EDS can only reflect the element content of a micro-area, and is a rough semi-quantitative analysis tool. Obviously, the combustion method is more accurate. For Figure S10c, the elemental content of the samples has determined by combustion method. It can be seen that with the increase of PVP dosage, the nitrogen atom content increased significantly. When the dosage of PVP is 40 %, the nitrogen content measured by combustion method rises sharply 3.81%, which can be attributed to the incomplete pyrolysis of PVP. This result corresponds to the residual polymer observed in the SEM image of NPGF-40 (Figure S8f).

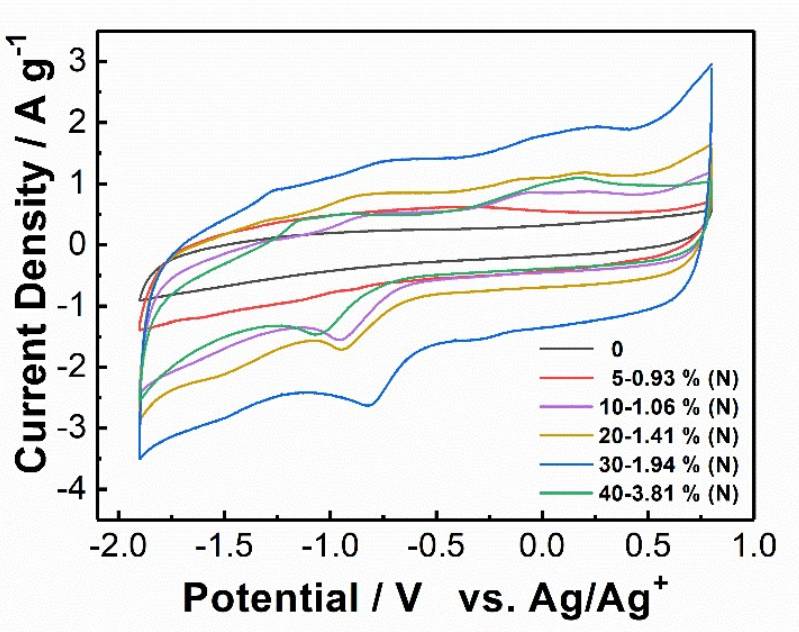

Figure S11. CV curves of NPGFs prepared with different PVP dosage.

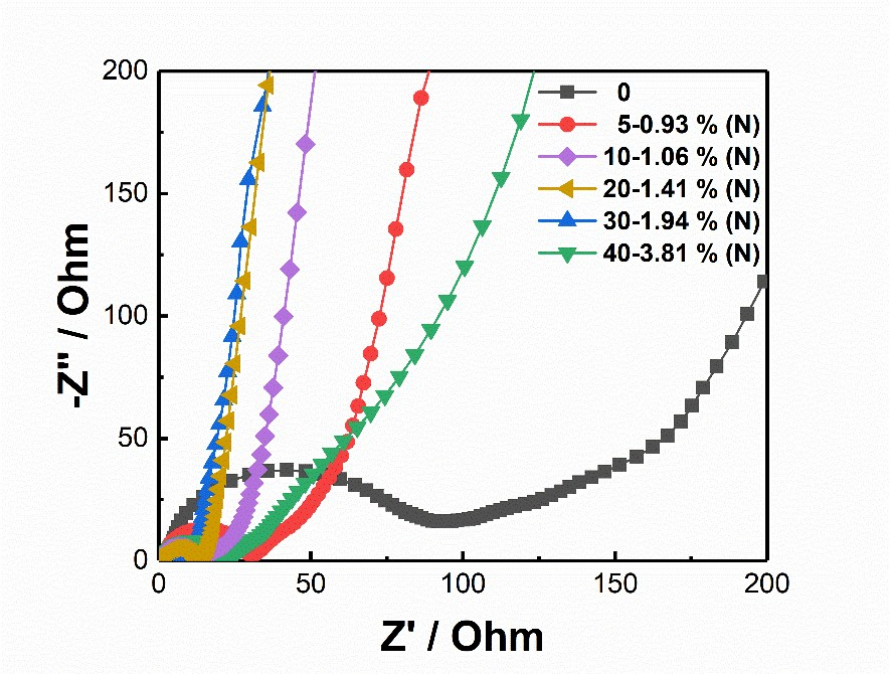

Figure S12. EIS of NPGFs prepared with different PVP dosage.

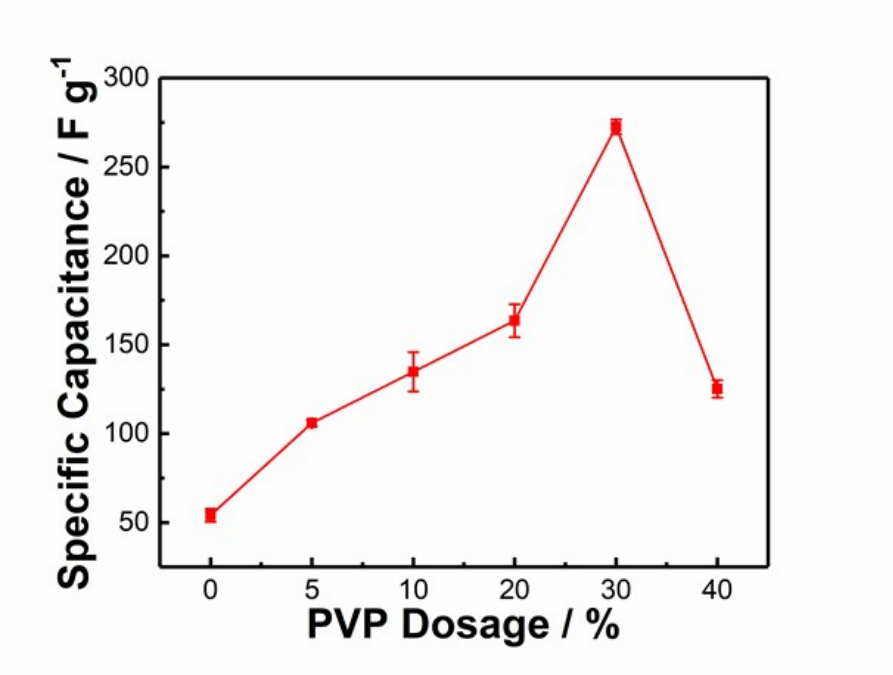

Figure S13. Specific capacitance of NPGFs at 2 A g^{-1} prepared with different PVP dosage.

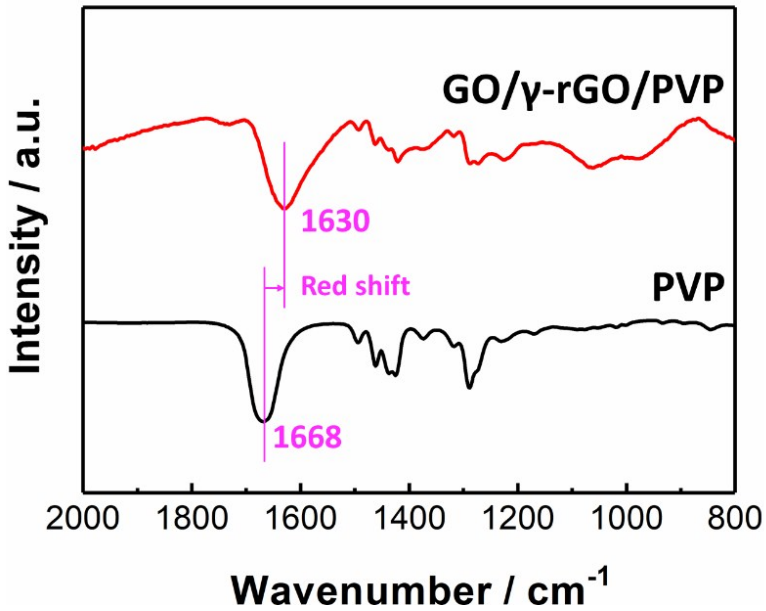

Figure S14. FTIR spectra of GO/γ-rGO/PVP and PVP.

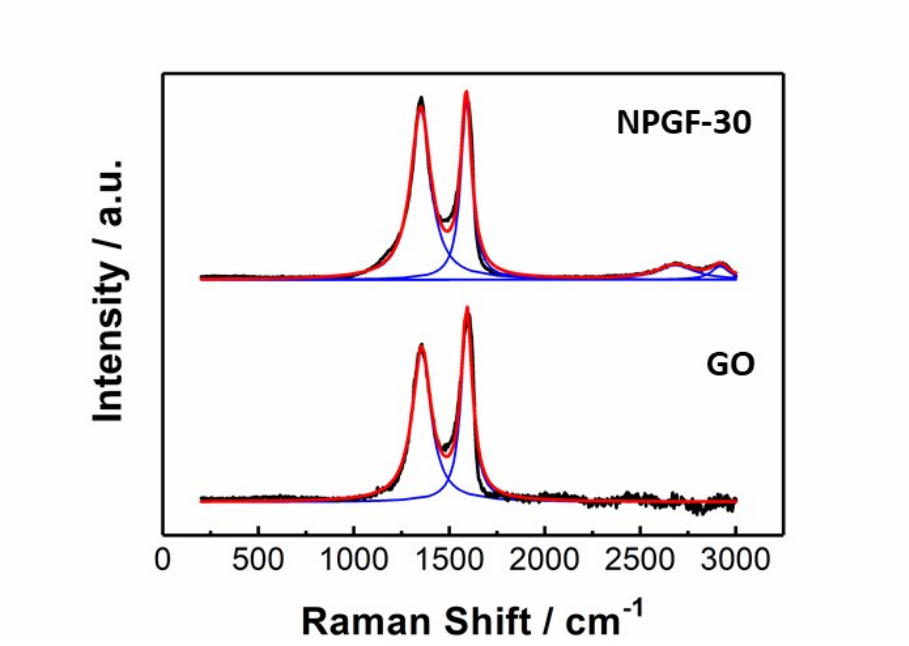

Figure S15. Raman spectra of GO and NPGF-30.

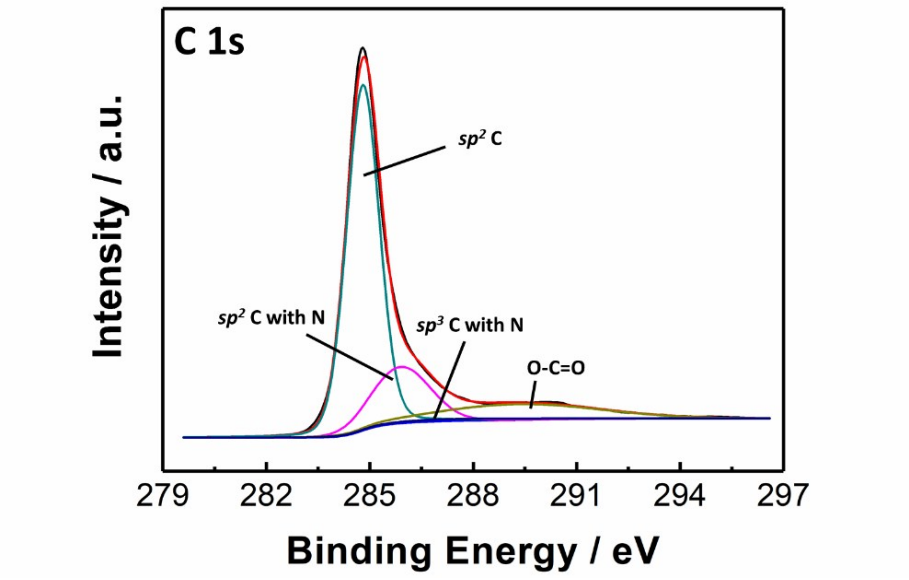

Figure S16. C 1s spectra of NPGF-30.

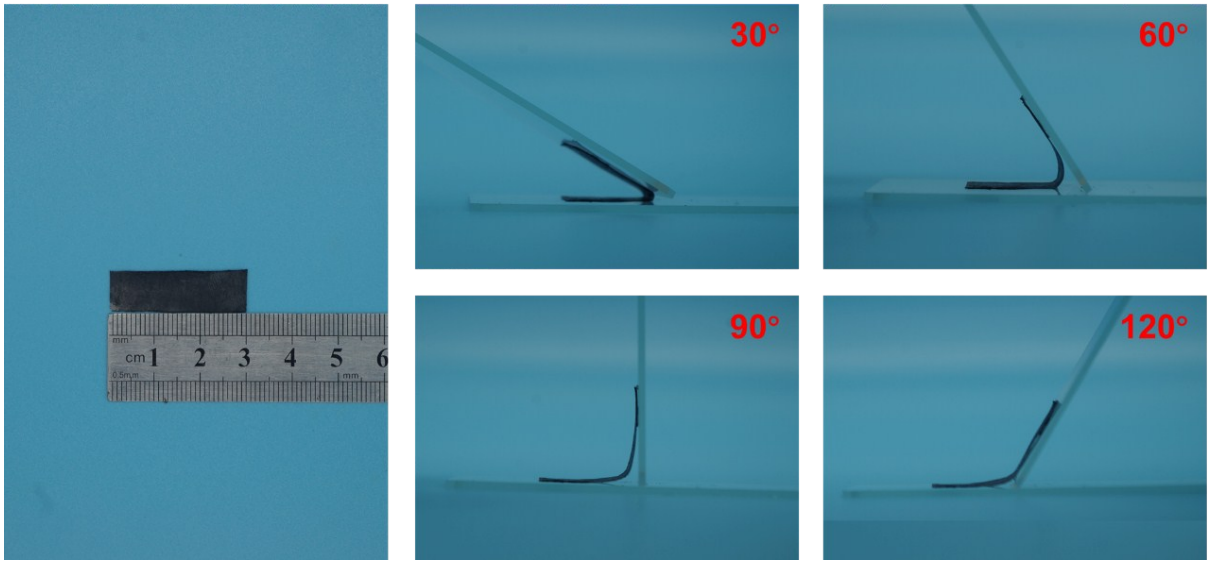

Figure S17. Digital photos of film-like NPGF-30 at different bending angles.

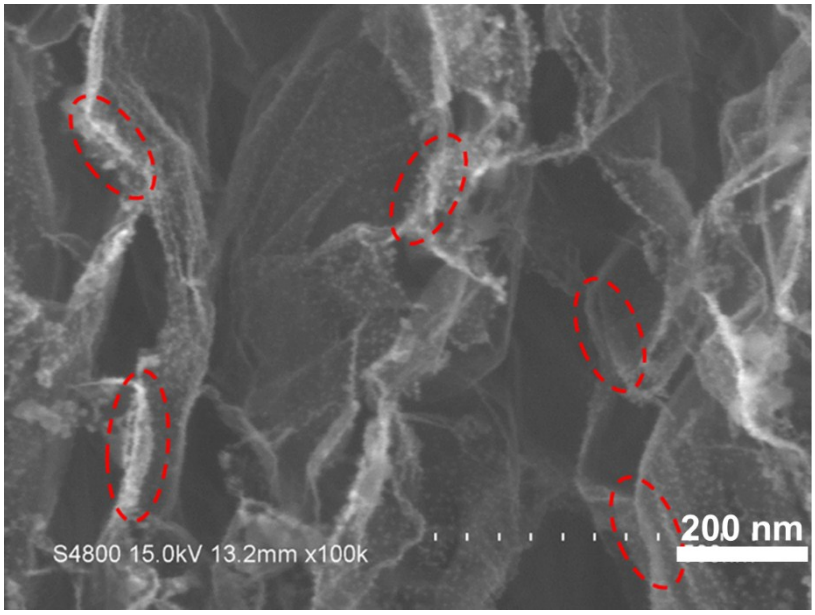

Figure S18. The cross-sectional FESEM image of aerogel-like NPGF-30 marked with conjugate regions.

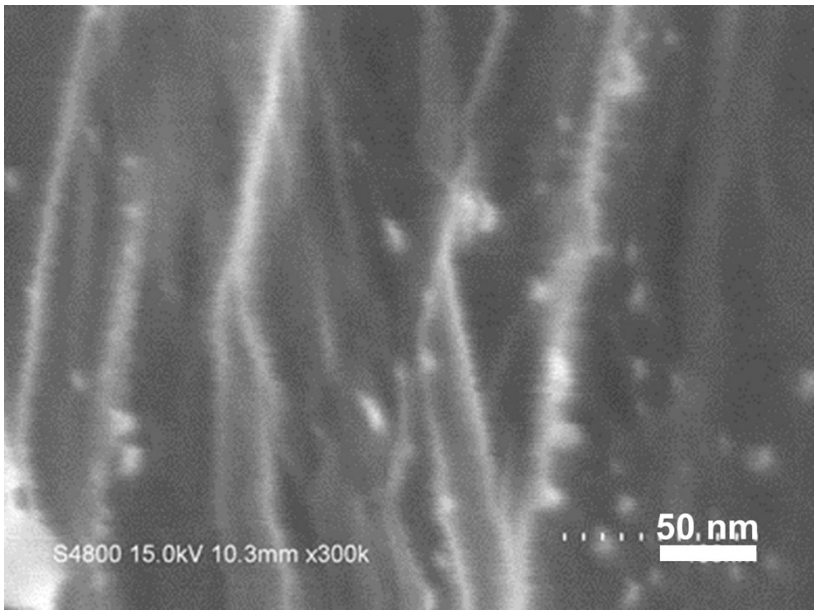

Figure S19. High-magnification FESEM images of film-like NPGF-30.

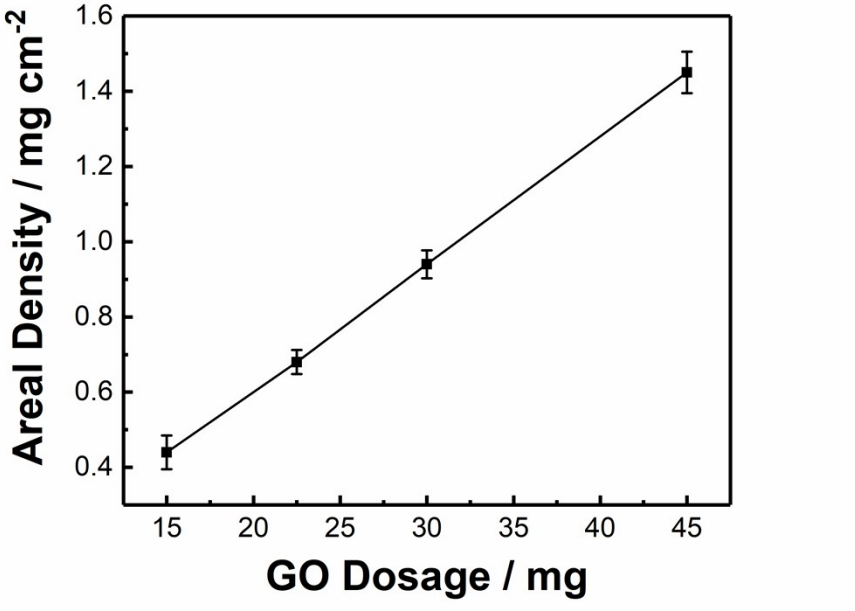

Figure S20. The areal density (areal mass loading) of NPGF-30 with different GO dosage.

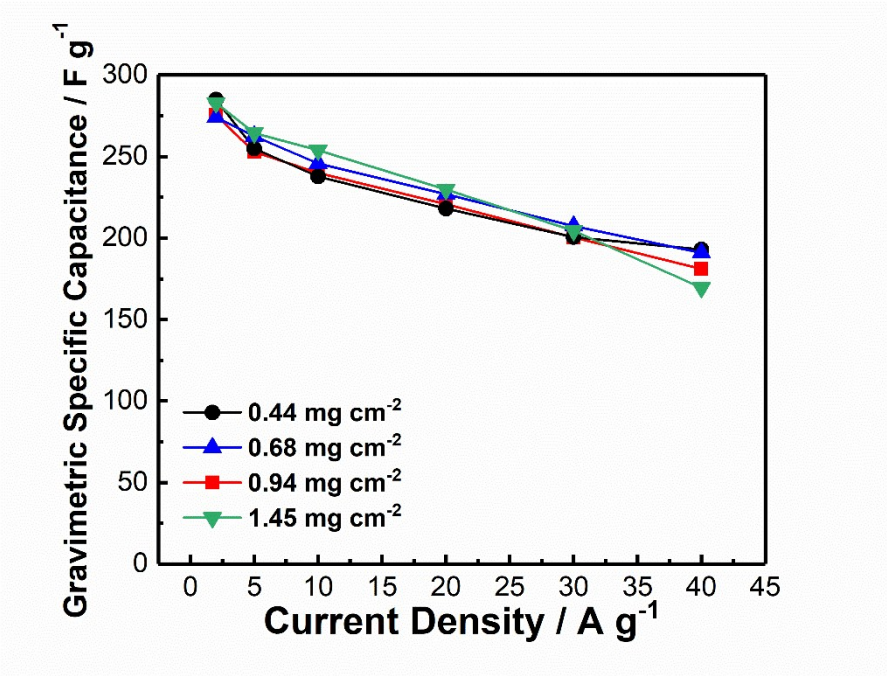

Figure S21. The gravimetric specific capacitance of NPGF-30 with different areal mass loading at different current densities.

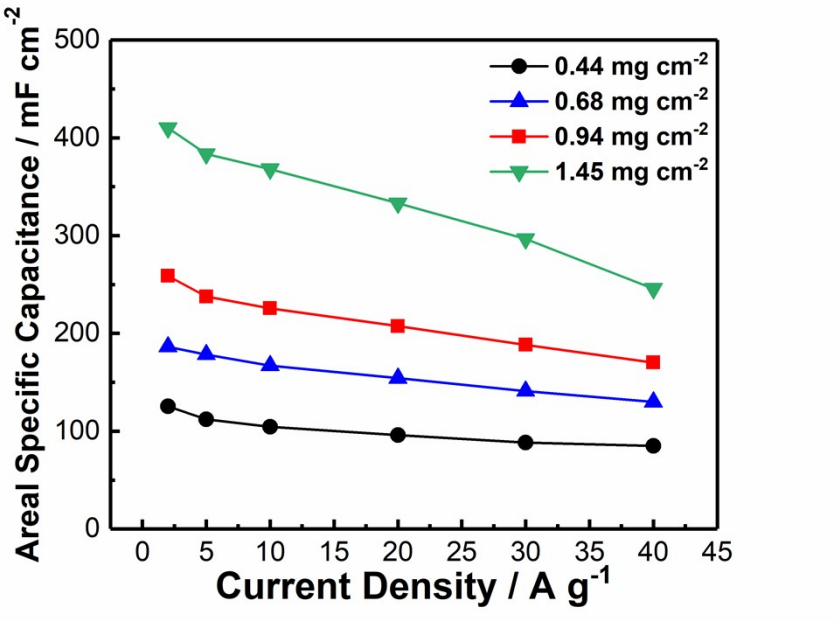

Figure S22. The areal specific capacitance of NPGF-30 with different areal mass loading at different current densities.

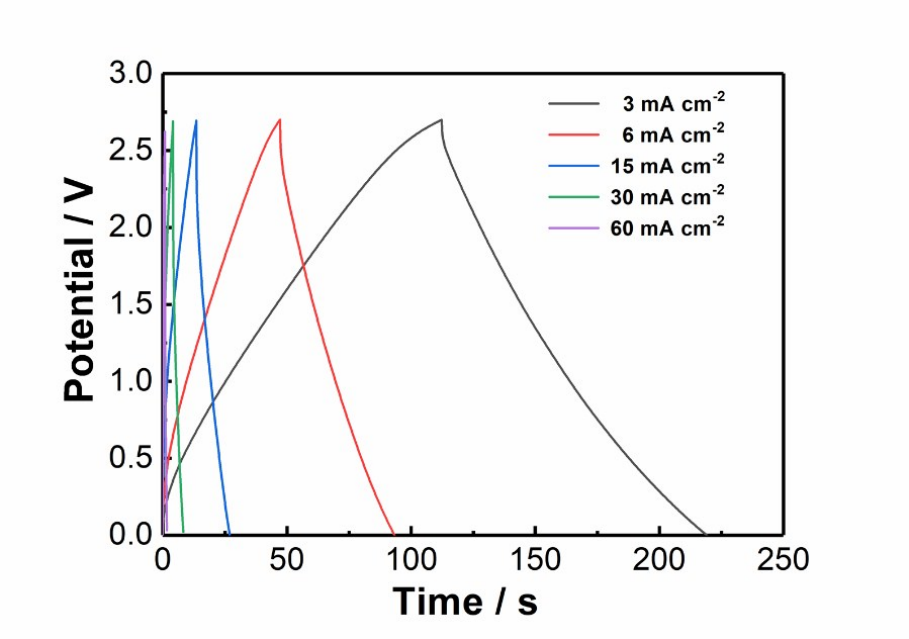

Figure S23. GCD curves of *o*CSC-30 at different current densities.

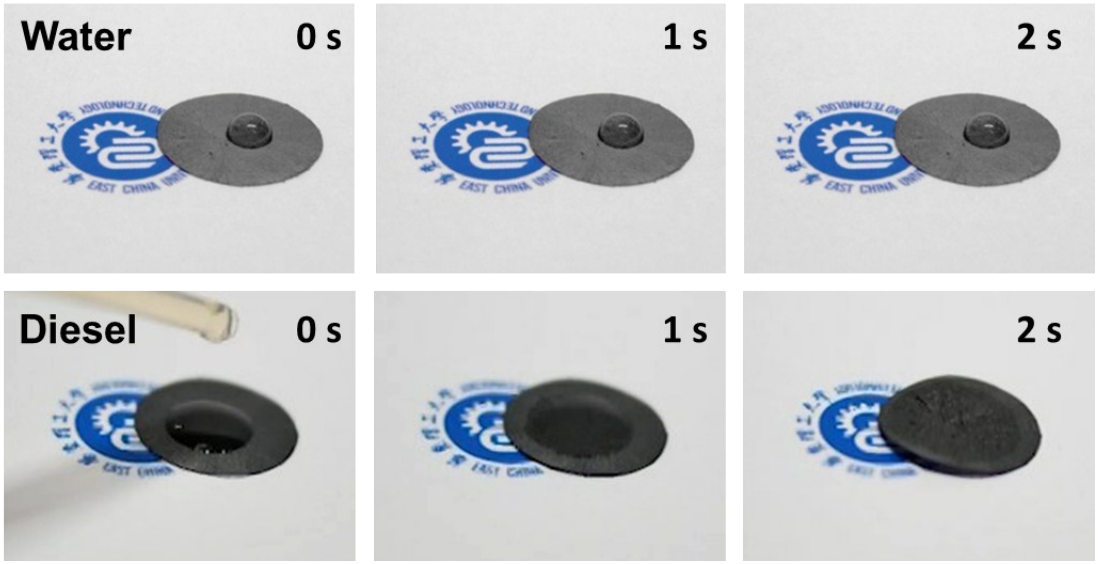

Figure S24. Video screenshots of changes in 2 s after dropping water and diesel oil onto the film-like NPGF-30, respectively.

Figure S25. Screenshots of the video showing film-like NPGF-30 immersed in water.

Table S1 The performance comparison of graphene-based supercapacitors.

References	Electrolyte	Potential Window	Energy density	Corresponding Power Density
this work	1 M Et_4NBF_4-AN	2.7 V	12.3 mWh cm^{-3} / 66.3 Wh kg^{-1}	0.42 W cm^{-3} / 2.2 kW kg^{-1}
49	Pyr_{14}TFSI/PVDF-*co*-HFP	3.5 V	16.5 Wh kg^{-1}	26.4 kW kg^{-1}
63	PVA-H_2SO_4	1.0 V	1.7 mW h cm^{-3}	60 mW cm^{-3}
64	$LiClO_4$-EC/DMC	3.0 V	30.0 Wh kg^{-1}	2.1 kW kg^{-1}
65	6 M KOH	1.0 V	12.5 Wh kg^{-1}	88.9 W kg^{-1}
66	PVA-H_2SO_4	1.0 V	2.78 mWh cm^{-3}	40.3 mW cm^{-3}
67	H_2SO_4	1.0 V	1.24 mWh cm^{-3}	0.89 W cm^{-3}
68	PVA-H_3PO_4	1.0 V	3.5 Wh kg^{-1}	28.1 kW kg^{-1}
69	6 M KOH	1.0 V	21.1 Wh kg^{-1}	5 kW kg^{-1}
70	PVA-H_2SO_4	1.0 V	552.3 μWh cm^{-3}	561.9 mWcm^{-3}
71	PVA-H_3PO_4	1.0 V	0.260 Wh L^{-1}	14.3 kW L^{-1}
72	1.5 M TEA-BF_4/AN	2.7 V	2.5 mWh cm^{-3}	40 Wcm^{-3}